THE JOURNAL OF PHYSICAL CHEMISTRY A

Article

pubs.acs.org/JPCA

The Role of Rydberg–Valence Coupling in the Ultrafast Relaxation Dynamics of Acetone

Markus Koch,* Bernhard Thaler, Pascal Heim, and Wolfgang E. Ernst

Institute of Experimental Physics, Graz University of Technology, Petersgasse 16, 8010 Graz, Austria

ABSTRACT: The electronic structure of excited states of acetone is represented by a Rydberg manifold that is coupled to valence states which provide very fast and efficient relaxation pathways. We observe and characterize the transfer of population from photoexcited Rydberg states (6p, 6d, 7s) to a whole series of lower Rydberg states (3p to 4d) and a simultaneous decay of population from these states. We obtain these results with time-resolved photoelectron–photoion coincidence (PEPICO) detection in combination with the application of Bayesian statistics for data analysis. Despite the expectedly complex relaxation behavior, we find that a simple sequential decay model is able to describe the observed PEPICO transients satisfactorily. We obtain a slower decay (~320 fs) from photoexcited states compared to a faster decay (~100 fs) of states that are populated by internal conversion, demonstrating that different relaxation dynamics are active. Within the series of Rydberg states populated by internal conversion, the decay dynamics seem to be similar, and a trend of slower decay from lower states indicates an increasingly higher energy barrier along the decay pathway for lower states. The presented results agree all in all with previous relaxation studies within the Rydberg manifold. The state-resolved observation of transient population ranging from 3p to 4d can serve as reference for time-dependent simulations.

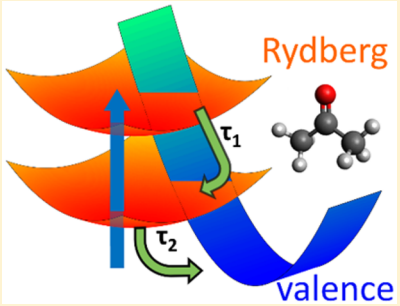

INTRODUCTION

The coupling of Rydberg and valence states provides efficient relaxation pathways for photoexcited molecular systems and has been the subject of many experimental and theoretical studies.[1−6] Acetone, being a prototype ketone molecule, is characterized by a series of parallel Rydberg state potentials converging to the ionic ground state, as indicated in Figure 1. These Rydberg states interact strongly with valence states,[4−6] resulting in very efficient relaxation pathways for nonradiative de-excitation through internal conversion (IC).

The relaxation and fragmentation dynamics in acetone, being among the most comprehensively studied photochemical processes,[7] have been thoroughly investigated by femtosecond time-resolved experiments. Most studies concentrate on the dynamics triggered by photoexcitation of the first excited state (S_1, corresponding to n → π^* excitation, see for example refs 8 and 9), or the lowest Rydberg state (S_2, n → 3s, see for example refs 10 and 11), for both of which relaxations do not proceed via Rydberg–valence interactions. Dynamics initiated by photoexcitation of the 3p and 3d Rydberg states, by contrast, show that nonradiative deactivation and corresponding fragmentation pathways are governed by Rydberg–valence coupling.[12−14,5] The interplay of Rydberg and valence states becomes even more important for excitation to higher Rydberg states above 3d, for which fewer experimental results are available.[13,15,16]

The unequivocal interpretation of the photoelectron (PE) and photoion transients turns out to be difficult or even impossible in this energy region because many parallel relaxation pathways can be active. Recently, the application of photoelectron–photoion coincidence (PEPICO) detection for time-resolved photoionization experiments[12,15,17,18] has proven to provide crucial experimental information, which allows one to disentangle parallel relaxation pathways and follow their temporal evolvement and fragmentation behavior. In a recent time-resolved PEPICO study with photoexcitation to the 5d to 6d Rydberg states, we were able to identify an IC relaxation pathway that transfers population to the 3p states.[15] However, no information could be obtained about the role of states between 3p and 5d. Other experiments targeting these higher Rydberg states also observe population decay through IC, but the reported time scales vary from 50 to 400 fs, resulting in different interpretations concerning the relaxation pathways.[12−14,5] Since these experiments differed in terms of their excitation conditions, the inconsistent results suggest that the relaxation dynamics depend sensitively on excitation parameters such as the exact photon energy or one- vs two-photon excitation. Therefore, a conclusive picture describing the exact relaxation pathways and the corresponding temporal behavior could not be obtained for excitation to states above 3p so far.

Most studies applied a two-photon excitation scheme to populate these high-lying Rydberg states, by combining ~4.5 eV pump and ~3.0 eV probe photon energies. With this combination two additional problems arise: (1) The simultaneous presence of the pump and probe photons activates an additional ionization channel, that overshadows all other transient signals and thereby covers the most interesting time interval of about 0−300 fs, where the majority of the

Received: May 24, 2017
Revised: July 18, 2017
Published: July 24, 2017

DOI: 10.1021/acs.jpca.7b05012
J. Phys. Chem. A 2017, 121, 6398−6404

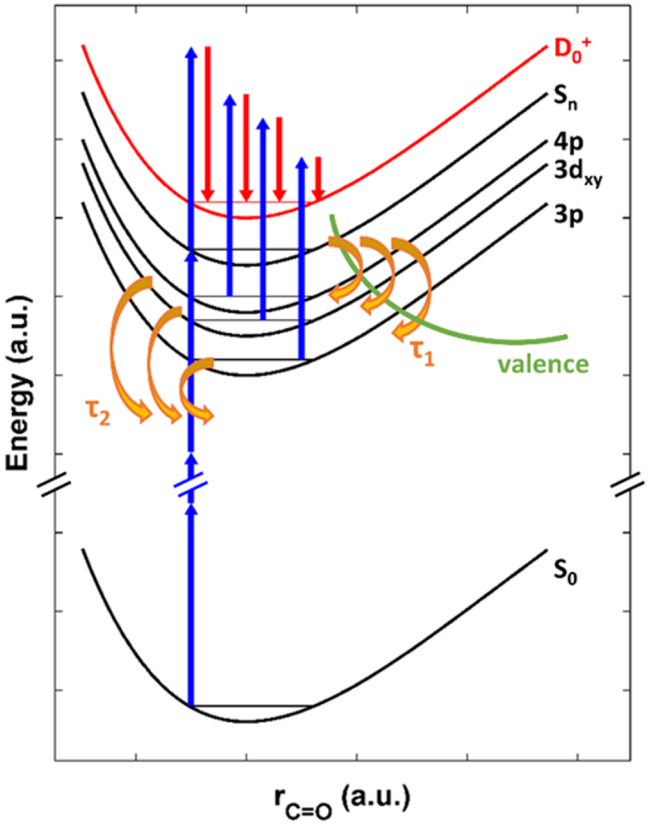

Figure 1. Schematic representation of the pump−probe experiment. Three-photon pump excitation (3.14 eV photon energy) is followed by time-delayed single-photon probe ionization (also 3.14 eV photon energy). If IC from the photoexcited S_n (6p, 6d, 7s) Rydberg states to lower Rydberg states occurs, the corresponding PE kinetic energy is reduced (red arrows). Population is transferred to these lower states with a time constant τ_1 and then further decays to lower states with a state dependent time constant τ_2.

population transfer occurs. (2) The pump photon energy enables two excitation pathways, one via two photon excitation directly to Rydberg states and one via resonant S_1 excitation in combination with fast geometry relaxation[19] and subsequent absorption of a second photon to different states. This leads to an unclear initial population distribution influencing the interpretation of relaxation dynamics. Only one study implemented the combination of single photon excitation using extreme ultraviolet pulses obtained from high-order harmonic generation with PEPICO detection.[12] The significant technical effort provides better control of the excitation and detection processes.

With a recent resonance-enhanced multi photon ionization (REMPI) study with single femtosecond laser pulses in the range of 3 eV photon energy,[17] we were able to resolve and assign PE bands to individual s, p, and d states of the Rydberg manifold ranging from 3p to 8s.

Here we present a time- and state-resolved investigation of the Rydberg state population in the range of 3p to 7s by applying pump and probe pulses with the same photon energy of 3.14 eV. We are able to observe the flow of population downward of the Rydberg manifold within the most interesting temporal region of 0−1.5 ps, without concealments due to parallel excitation pathways or overwhelmingly strong pump−probe cross correlation signals. In the following, we first describe the experimental methods and the sequential fitting model, before we present the PEPCIO transients and a discussion of their interpretation.

METHODS

The setup has been described in more detail previously.[15] In brief, a commercial Ti:sapphire laser system (Coherent Vitara oscillator and Legend Elite Duo amplifier) was used delivering pulses with 800 nm center wavelength, 25 fs pulse duration, and 4 mJ pulse energy, at a 3 kHz repetition rate. The laser output was split into a pump and a probe pulse with a variable pump−probe time delay. The pump and probe pulses were frequency doubled in two separate BBO crystals to obtain 3.14 eV photon energies (395 nm center wavelength) with a spectral bandwidth of ∼40 meV. Pump and probe pulses were focused with a 500 mm lens into the vacuum chamber, where they overlapped in the extraction region of the PEPICO spectrometer. The pulse duration and chirp were checked by frequency resolved optical gating,[20] and the temporal resolution of the setup was determined from the pump−probe cross correlation signals (see below) to be (84 ± 1) fs full width at half-maximum.

Acetone (purity: >99.9%) was introduced into the vacuum chamber (<5×10^{-10} mbar base pressure) at a partial pressure of typically 5×10^{-6} mbar. Coincidence detection of ions and electrons was achieved by a single 0.5 m time-of-flight spectrometer with a pulsed extraction field. For electrons a magnetic bottle configuration in combination with a small extraction voltage (−3 V) was used, with an estimated energy resolution of $\Delta E/E$ = 4%.[21] The ions were extracted by applying a high voltage pulse (+2 kV) to the repeller electrode about 100 ns after the laser pulse. Signal pulses were decoupled from the anode of a microchannel plate detector, digitized by a high-speed analog-to-digital converter card (Gage Cobra, Dynamic Signals LLC), and analyzed by a coincidence algorithm.

The intensities of the pump and probe pulses and the acetone particle density were chosen in order to keep false coincidences at a low rate. The three photon excitation results in an unavoidable high pump-only background which spectrally overlaps with the pump−probe signal.[17] Since simple subtraction of these two almost equally strong signals would result in a poor signal-to-noise ratio, the true pump−probe signal was calculated with Bayesian probability theory,[22] enhancing the signal-to-noise ratio significantly, especially at long pump−probe delays where the signal from the excited states is low.

We consider a sequential decay model where a fraction N_0 of the ground state population is photoexcited to an excited state $|1\rangle$ by a pump pulse, which has a Gaussian temporal shape $g(t) = \frac{N_0}{\sigma\sqrt{2\pi}} \exp\left(-\frac{t^2}{2\sigma^2}\right)$, with the standard deviation σ. Population N_1 decays from state $|1\rangle$ into state $|2\rangle$ with the time constant τ_1, and population N_2 decays to lower states with the time constant τ_2. The dynamics can be described by two coupled differential equations:

$$\frac{dN_1}{dt} = -\frac{N_1}{\tau_1} + g(t)$$

$$\frac{dN_2}{dt} = -\frac{N_2}{\tau_2} + \frac{N_1}{\tau_1}$$

The solutions are

DOI: 10.1021/acs.jpca.7b05012
J. Phys. Chem. A 2017, 121, 6398−6404

$$N_1(t) = N(t, \tau_1) \quad (1)$$

$$N_2(t) = \frac{\tau_2}{\tau_2 - \tau_1}[N(t, \tau_2) - N(t, \tau_1)] \quad (2)$$

with

$$N(t, \tau) = \frac{N_0}{2}\exp\left(\frac{\sigma^2}{2\tau^2}\right)\left[1 + \mathrm{erf}\left(\frac{t - \frac{\sigma^2}{\tau}}{\sigma\sqrt{2}}\right)\right]\exp\left(\frac{-t}{\tau}\right) \quad (3)$$

where $\mathrm{erf}(x)$ is the error function, which is shifted in time by $\frac{\sigma^2}{\tau}$. For $\sigma \ll \tau$ eq 3 becomes $N(t, \tau) = N_0 H(t)\exp\left(\frac{-t}{\tau}\right)$, where $H(t)$ is the Heaviside step function, a model that has been frequently used for nonadiabatic decay dynamics.[23] Note that this fit model also applies if several lower states are filled simultaneously, where the population of all lower states increases with τ_1 and the different coupling efficiencies to state $|1\rangle$ are represented by corresponding amplitudes.

The equal pump and probe photon energies additionally cause a pump−probe cross correlation signal that is accounted for by superimposing a Gaussian peak with the same standard deviation σ as the excitation pulse above. The maximum of the cross correlation signal defines time zero. The populations $N_1(t)$ and $N_2(t)$ together with the cross correlation signal are fitted to the parent and fragment PEPICO transients.

RESULTS AND DISCUSSION

The highest occupied molecular orbital (HOMO) of acetone can primarily be described as lone pair at the oxygen atom with nonbonding character.[24] Photoexcitation to Rydberg states and photoionization of the HOMO electron does therefore not change the molecular geometry, resulting in a series of parallel potential energy surfaces (PES), as depicted in Figure 1.[4]

Couplings to valence states provide very fast and efficient relaxation pathways for population transfer to lower states[4−6] with a time constant τ_1. In a simultaneous process, population decays from different Rydberg states with individual decay times τ_2.

Photoexcitation with three 3.14 eV photons transfers population from the ground state to a group of Rydberg states S_n (6p, 6d, 7s) which lie within the laser bandwidth (see Figure 1). PEPICO spectra obtained by ionization with a time-delayed probe pulse (also 3.14 eV photon energy) are shown in Figure 2 for three characteristic delay times. The PEPICO technique allows one to separately display the PE spectrum detected in coincidence with the acetone parent ion (Figure 2a) and in coincidence with the acetyl fragment ion (Figure 2b). From these spectra an allocation of PE bands to a series of Rydberg states within the whole temporal range from 0 to 1.5 ps pump−probe delay is possible. This assignment is crucial to obtain the presented interpretation and was not possible in our previous study,[15] which we attribute to the choice of photon energies (3.1 eV instead of previously 4.6 eV) and the application of Bayesian probability theory for background subtraction. Because of PEPICO detection we obtain direct information about the relaxation dynamics, as well as the fragmentation behavior. The spectral signatures of Figure 2 are in line with our previous interpretation of single-pulse REMPI experiments.[17] The individual PE peaks can be assigned to the *n*s, *n*p, and *n*d Rydberg series (Figure 2b), based on comparison with accurate synchrotron experiments,[25,26] as explained in more

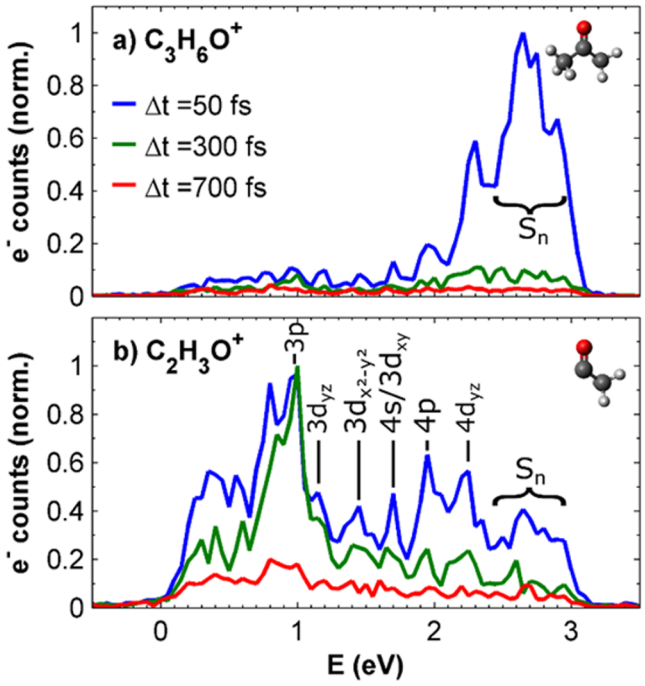

Figure 2. Photoelectron kinetic energy spectra in coincidence with parent ions (a) and with acetyl fragment ions (b) for different pump−probe time delays Δt. PE bands of the fragment PEPCIO spectrum can be assigned to a series of acetone Rydberg states,[17] as indicated. The parent and fragment spectra are separately normalized.

detail in our previous work.[17] In addition to the previous assignment we note that for the 3p band the CO stretch vibrational progression can be observed as lower energy side peaks separated by 0.18 eV.[6,13] The PE peaks below the excited S_n states prove that ultrafast relaxation transfers population to lower states. Ionization from higher Rydberg states (above ∼2 eV, corresponding to the 4p state) leads predominantly to parent ions, while ionization from lower states yields fragmentation. The fragmentation process takes place after ionization in the ionic ground state as proven by the assignment of fragment PEPICO peaks to Rydberg states of unfragmented acetone. Energy conversion from electronic to vibrational energy during the relaxation process is responsible for fragmentation, for which the activation energy threshold was determined to be (0.79 ± 0.04) eV.[17]

PEPICO spectra for three selected delays of 50, 300, and 700 fs are shown in Figure 2. While a complete picture of the relaxation dynamics is revealed below by analysis of a full time-delay scan, a discussion of these selected spectra is instructive as it provides a first insight into the population transfer. During temporal overlap of pump and probe pulses (50 fs delay) a very strong parent PEPICO signal (Figure 2a, blue curve) is observed. This rapidly decreasing signal represents the pump−probe cross correlation due to equal photon energies of pump and probe pulses. A slower decaying component, which is indeed observed in the parent PEPICO transient (see below), is weakly indicated by the 300 fs spectrum (green). Concerning the fragment spectra, two important aspects are to be mentioned: (1) The spectrum at 50 fs pump−probe delay (Figure 2b, blue curve) shows strong PE bands that can be assigned to a series of Rydberg states down to the 3p state. This indicates that significant population transfer to these states occurs within the first 50 fs and that the corresponding filling

DOI: 10.1021/acs.jpca.7b05012
J. Phys. Chem. A 2017, 121, 6398−6404

time constant is the same for all lower states populated by IC. (2) The 50 fs (blue) and 300 fs (green) spectra are all in all very similar and the signal has not significantly dropped, in particular for the 3p and 3d states. This shows that population transfer from S_n to these states remains active after about 300 fs and that population decay from these states proceeds with time constants on the order of a few hundred femtoseconds. Furthermore, there is a trend of stronger signal decrease of higher states (4p, $4d_{yz}$) and weaker decrease of lower states (3p, 3d), suggesting that the decay from higher states proceeds faster compared to lower states. At 700 fs the PE signal has significantly decreased. Finally, we note that the fragment PEPICO signal assigned to the S_n states at 2.4−3.1 eV is caused by ionization to the ionic ground state in combination with fragmentation due to subsequent excitation of the ion, as demonstrated by previous laser intensity scans.[17] The PE bands below 0.5 eV cannot be assigned and might be related to valence states.[17]

To obtain deeper insight into the population transfer dynamics we recorded the full time-resolved PE spectra associated with the parent (Figure 3a) and fragment (Figure 3b) ions. The parent PEPICO signal is confined to the small energetic region of the photoexcited S_n band, and its fast decay reflects the pump−probe cross correlation. The overall width and rich structure of the fragment PEPICO signal reaching from 0 to 3 eV, in contrast, represents population in the corresponding Rydberg states, as assigned in Figure 2b. Also, the longer lasting ion signal from these states is evident, in particular at about 1 eV, which is visible for about 500 fs.

To model the population transfer between the Rydberg states as a function of time we integrate the signal within energy regions assigned to individual states, as indicated by vertical color bars in Figure 3. The obtained state-resolved parent and fragment PEPICO transients are shown in Figure 4, plotted with the same color assignment. These transients contain two contributions: (1) the important temporal change representing the population transfer between the Rydberg states and (2) the Gaussian peak due to the pump−probe cross correlation. The parent PEPICO transient (Figure 4a) shows a single exponential decay, caused by the decay of population from the photoexcited S_n states. The fragment PEPICO transients (Figure 4b), by contrast, reveal a fundamentally different temporal behavior, representing the sequential decay model. They increase to a maximum at about 250 fs and then decay to zero. The rising and falling character is caused by the initial population increase due to filling from S_n and simultaneous population decay, respectively. These results confirm the initial interpretation of the fragment PEPICO spectra (Figure 2) above.

We fit the decay model introduced in eqs 1−3 to the transient PEPICO spectra in order to develop a quantitative

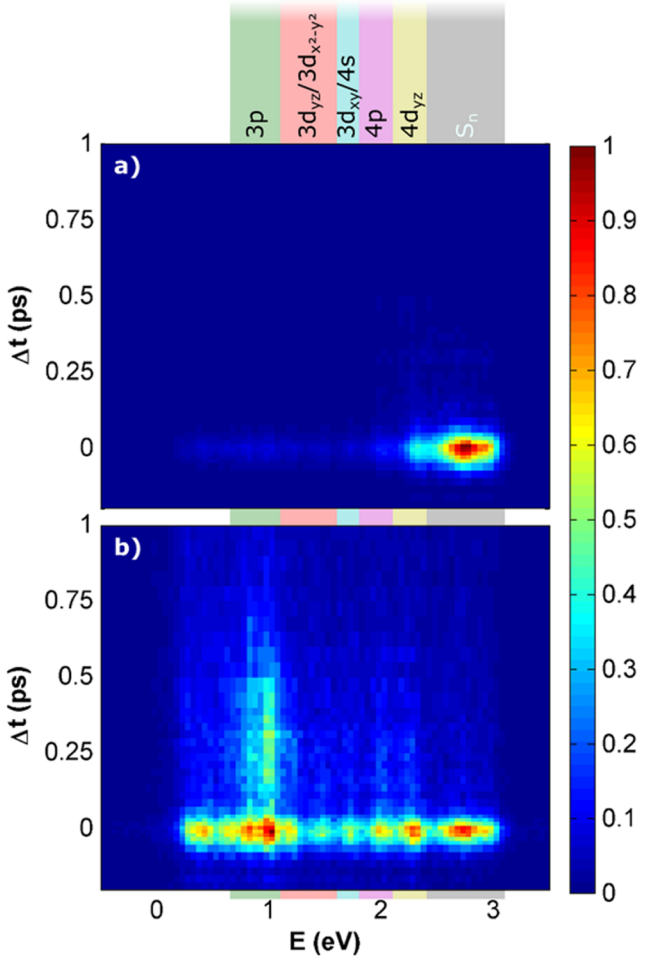

Figure 3. Time-resolved parent (a) and fragment (b) PEPICO spectra, plotted with an energy resolution of 50 meV. Energy ranges that are integrated for state-resolved transient signals (Figure 4) are marked with colors and labeled at the top (3p, 0.65−1.1 eV (green); $3d_{yz}$/$3d_{x^2-y^2}$, 1.1−1.6 eV (red); $3d_{xy}$/4s, 1.6−1.8 eV (cyan); 4p, 1.8−2.1 eV (magenta); $4d_{yz}$, 2.1−2.4 eV (yellow); S_n, 2.4−3.1 eV (black)).

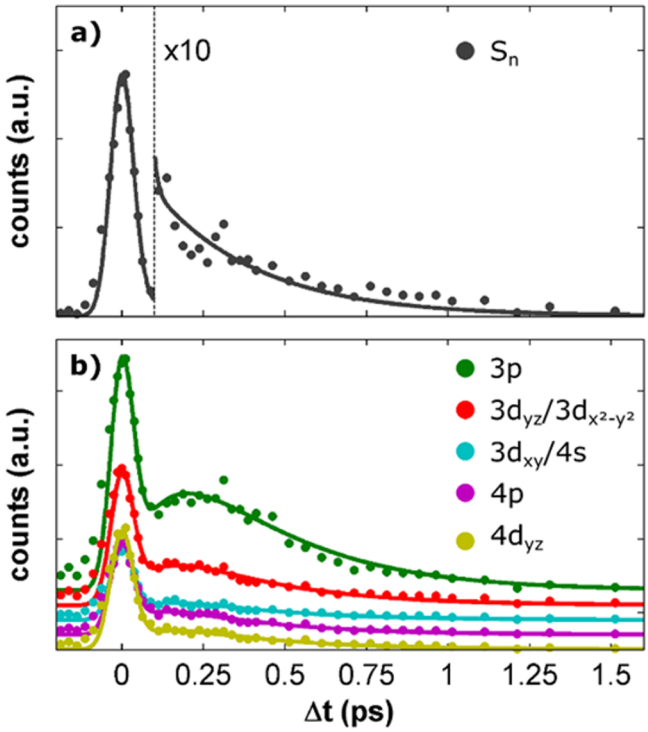

Figure 4. Parent (a) and fragment (b) PEPICO transients, assigned to different Rydberg states, as given in the legend. The signals are obtained by integrating the time-resolved PEPICO signals within the corresponding energy regions, which are indicated by the same colors as in Figure 3. Solid lines represent the fit results of eqs 1−3 with the obtained parameters as listed in Table 1. For visibility, the curves are vertically offset.

DOI: 10.1021/acs.jpca.7b05012
J. Phys. Chem. A 2017, 121, 6398−6404

Table 1. Decay Time Constants τ for Different Rydberg States, as Obtained by This Work via the Sequential Fit Model, Eqs 1−3, and by Previous Experiments[a]

			τ/fs						
state	sym	E[25]/eV	this work	Maierhofer et al.[15]	Rusteika et al.[16]	Hüter et al.[13]	Couch et al.[12]	Sølling et al.[5]	Farmanara et al.[14]
$3p_x$	A_1	7.34	τ_2 = 128 ± 13	(141 ± 14)[b]	250	(280 ± 40) to (710 ± 40)	330 ± 30		
$3p_y$	A_2	7.41							
$3p_z$	B_2	7.45							
$3d_{yz}$	A_1	7.72	τ_2 = 96 ± 17			(50 ± 5) to (90 ± 5)	<50	<60	330 ± 40
$3d_{x^2-y^2}$	B_2	8.09							
$3d_{xy}$	B_1	8.17	τ_2 = 87 ± 33						
4s	B_2	8.22							
4p	A_1	8.58	τ_2 = 73 ± 23						
$4d_{yz}$	A_1	8.70	τ_2 = 81 ± 29		250				
S_n (6p, 6d, 7s)		9.30	τ_1 = 319 ± 23	154 ± 44					
excitation energy/eV			3 × 3.14 = 9.42	2 × 4.61 = 9.22	2 × 4.4 = 8.80	2 × (3.88 to 4.19) = (7.76 to 8.38)	8.00	2 × 4.04 = 8.08	8.00

[a]On the left the states are listed, including their symmetry (sym)[24] and energy E.[25] The states are grouped according to the energy ranges used for the fitting routine (see Figure 3), as indicated by blank rows in the table. In the last line the excitation energy of each experiment is listed. [b]The 3p decay time constant is obtained by averaging the parent and fragment PEPICO signals.

interpretation. We globally optimize the laser pulse duration, σ, and the decay time constant of state $|1\rangle$, τ_1, under the assumption that the time constant for population increase of all lower Rydberg states (3p to $4d_{yz}$) is the same as that for population decrease of the photoexcited S_n state. In other words, population is assumed to be transferred directly from S_n to the lower states, without intermediate states being populated. Hence, both the decaying parent signal and the increasing fragment signals of all observed lower states are considered for the determination of τ_1. With the global least-squares approximation using a Levenberg−Marquardt algorithm we obtain σ = (35.6 ± 0.3) fs and τ_1 = (319 ± 23) fs.

The decay time constant τ_2 is assumed to be state dependent and is therefore determined separately for each energy range of the fragment PEPCIO signal (cf. Figure 3). The τ_1 and τ_2 decay times are listed in Table 1, and corresponding fit curves are drawn as solid lines in Figure 4. The good agreement between the transient signals and our simple model demonstrates that the majority of the photoexcited population follows a sequential decay. In general, however, it could be expected that relaxation pathways with a different, nonsequential behavior are active, which deviate, for example, from the assumed simultaneous decrease of the photoexcited states and increase of the lower states. The contribution of such channels is not recognized in our transients (Figure 4). We also note that a very fast decay of the S_n states with a time constant below ∼100 fs would probably be hidden by the pump−probe cross correlation peak (Figure 4a). However, a fast population increase in the lower states (Figure 4b) should be present, which is not the case, as the signal increases to a maximum at 250 fs.

It is also important to note that, due to PEPICO detection, we can exclude fragmentation in the neutral because all the observed bands in the spectra can be assigned to the unfragmented parent molecule.

In the following we discuss the obtained state-dependent decay time constants, which are summarized in Table 1, and compare them to the results of previous experiments. For the states of the Rydberg manifold that are populated by IC (3p to $4d_{yz}$) the decay times are all around 100 fs and a trend of slower decay from energetically lower states is observed. The decay time constant τ_2 is state dependent with a monotonic decrease by almost 50 fs for increasing state energy, from $\tau_{2,3p}$ = (128 ± 13) fs to $\tau_{2,4dyz}$ = (81 ± 29) fs. This relation is shown in Figure 5 as a function of the PE kinetic energy. It is surprising that the time constants of these states are similar because, first, the Rydberg−valence interaction would be expected to depend on the symmetry of the Rydberg state, as the lowest-energy valence state interacting with the Rydberg manifold, the $\pi\pi^*$ state, has A_1 symmetry[4,6] and the observed Rydberg states are of A_1, B_1, and B_2 symmetry (Table 1). Second, conical

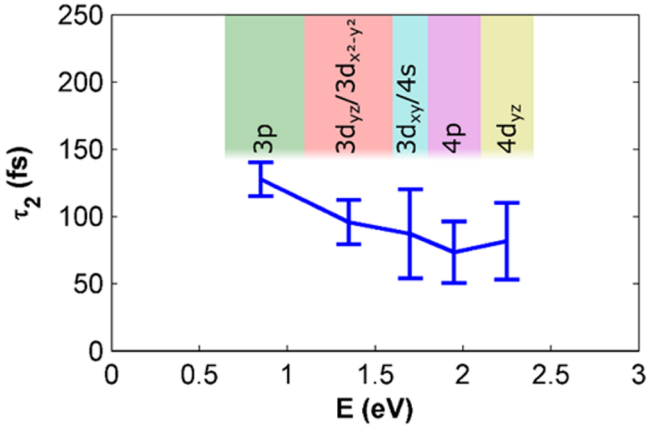

Figure 5. Decay time constant τ_2 as a function of the state energy E for Rydberg states populated by internal conversion.

DOI: 10.1021/acs.jpca.7b05012
J. Phys. Chem. A 2017, 121, 6398−6404

intersections (CI)[27] are generally involved in IC processes and the relaxation pathways of the wave packets at CIs are found to depend on various parameters such as its energetic location, its geometry, or how it is approached by the wave packet. The influence of CIs on different reaction channels is demonstrated, for example, in molecular photofragmentation, as observed by photofragment translational spectroscopy.[28,29] The yields of reaction products and their kinetic energies were found to depend, for example, on the nature of the photoexcited state,[3,30,31] the vibrational excitation,[32−35] or dynamic resonances.[36,37]

In this context, the similarity of the decay time constants τ_2 for different Rydberg states (Table 1 and Figure 5) indicates that similar dynamics are active during the relaxation of population from these Rydberg states. The monotonic increase of τ_2 for lower states implies that an increasing energy barrier is present along the IC reaction coordinate for decreasing state energy. This is supported by calculated excited-state PESs along the CO stretching coordinate[4] which show that the intersection point of valence and Rydberg states shifts relative to the PES minimum within the Rydberg manifold. While it is close to the PES minimum for states above 3d, it lies a few hundred millielectronvolts above the PES minimum for the 3p states.[4]

Our reported 3p decay time of τ_{3p} = (128 ± 13) fs is in line with previous results under the assumption that the decay time of a state depends on the energy difference between the photoexcited state and the decaying state. If the wave packet has gained more energy on its way to a certain lower state, it will be able to overcome a potential barrier more quickly. Couch et al.[12] observe a time constant of (330 ± 30) fs for the 3p decay upon a one-photon excitation with 8.0 eV photon energy (see Table 1). Hüter et al.[13] obtain a range between (710 ± 40) and (280 ± 40) fs for excitation energy between 7.76 and 8.38 eV. Considering that our excitation energy is 1.4 eV higher compared to these results, we conclude that our value supports the trend of shorter lifetimes for higher excitation energies.

Previously observed population decay from the $3d_{yz}$ state is somewhat more contradicting: Farmanara el al.[14] report a 330 fs decay, while Hüter et al.,[13] Couch et al.,[12] and Solling et al.[5] obtain much shorter time constants of (50 ± 5) to (90 ± 5) fs, <50 fs, and <60 fs, respectively. Our observed decay time constant lies with τ_{3dyz} = (96 ± 17) fs within the same range.

The time constant in connection with the decay of the photoexcited S_n states, τ_1 = (319 ± 23) fs, is significantly longer than any of the lower state time constants (3p to $4d_{yz}$). This observation is in agreement with the proposed trend of slower decay for less excess energy because photoexcited S_n population has not experienced conversion of electronic to kinetic energy through nonadiabatic relaxation. The value of (319 ± 23) fs is, however, in disagreement with our previous result of (154 ± 44) fs,[15] which was measured with two-photon excitation instead of the three-photon excitation of the present experiment. Due to the laser bandwidth several electronic states ($6p_x$, $6p_y$, $6p_z$, $6d_{xy}$, $6d_{yz}$, $6d_{xz}$, $6d_{x^2-y^2}$, $6d_{z^2}$, 7s) can be populated in this excitation region. These Rydberg states presumably provide different relaxation pathways with different decay time constants. As argued above, the activation of these pathways and, consequently, also the observed decay time are assumed to depend sensitively on the excitation conditions.[3,30−37]

SUMMARY AND CONCLUSION

We have measured the electronic relaxation dynamics in acetone molecules triggered by excitation to high-lying Rydberg states (7s, 6p, 6d). The population flow downward of the Rydberg manifold to the 3p states can be followed by observing the increase and decrease of PE bands corresponding to various different Rydberg levels. Despite the general complexity in relaxation dynamics caused by the involvement of CIs, we find that a simple sequential decay model describes the observed transient signals satisfactorily. Within this model, population undergoes IC from the photoexcited states to lower Rydberg states with a time constant of τ_1 = (319 ± 23) fs. For further decay the time constants are state dependent ranging from $\tau_{2,3p}$ = (128 ± 13) fs to $\tau_{2,4dyz}$ = (81 ± 29) fs, with a nearly monotonic decrease. The decay time difference between the photoexcited state and the lower Rydberg states that are populated by relaxation indicates that the dynamics of the IC processes are different. The dynamics during decay from the lower states ($4d_{yz}$ to 3p), in contrast, seem to be similar. Furthermore, an increasing barrier along the IC path for lower states would explain the observed monotonic decrease of the decay time.

While our simple model seems to well describe the relaxation behavior of the majority of the photoexcited population in the case of acetone, the actual relaxation dynamics within the Rydberg manifold mediated by valence states must be much more diverse and complex. A comprehensive description will only be possible with time-resolved simulations such as trajectory surface hopping,[38] for which our results can serve as reference.

AUTHOR INFORMATION

Corresponding Author

*E-mail: markus.koch@tugraz.at.

ORCID

Markus Koch: 0000-0003-0186-1614

Wolfgang E. Ernst: 0000-0001-8849-5658

Notes

The authors declare no competing financial interest.

ACKNOWLEDGMENTS

The authors acknowledge experimental support by Stefan Cesnik and Sascha Ranftl, and financial support by the Austrian Science Fund (FWF) under Grant P29369-N36, as well as support from NAWI Graz.

REFERENCES

(1) Champenois, E. G.; Shivaram, N. H.; Wright, T. W.; Yang, C.-S.; Belkacem, A.; Cryan, J. P. Involvement of a Low-Lying Rydberg State in the Ultrafast Relaxation Dynamics of Ethylene. *J. Chem. Phys.* **2016**, *144* (1), 014303−014303.

(2) Reisler, H.; Krylov, A. I. Interacting Rydberg and Valence States in Radicals and Molecules: Experimental and Theoretical Studies. *Int. Rev. Phys. Chem.* **2009**, *28* (2), 267−308.

(3) Rodrigo, C. P.; Zhou, C.; Reisler, H. *J. Phys. Chem. A* **2013**, *117* (46), 12049−12059.

(4) Diau, E. W. G.; Kötting, C.; Solling, T. I.; Zewail, A. H. Femtochemistry of Norrish Type I Reactions: III. Highly Excited Ketones-Theoretical. *ChemPhysChem* **2002**, *3* (1), 57−78.

(5) Solling, T. I.; Diau, E. W.-G.; Kötting, C.; De Feyter, S.; Zewail, A. H. Femtochemistry of Norrish Type I Reactions: IV. Highly Excited Ketones-Experimental. *ChemPhysChem* **2002**, *3* (1), 79−97.

DOI: 10.1021/acs.jpca.7b05012
J. Phys. Chem. A 2017, 121, 6398−6404

(6) Merchan, M.; Roos, B. O.; McDiarmid, R.; Xing, X. A Combined Theoretical and Experimental Determination of the Electronic Spectrum of Acetone. *J. Chem. Phys.* **1996**, *104* (5), 1791−1791.
(7) Haas, Y. Photochemical α-Cleavage of Ketones: Revisiting Acetone. *Photochem. Photobiol. Sci.* **2004**, *3* (1), 6−16.
(8) Diau, E. W.-G.; Kötting, C.; Zewail, A. H. Femtochemistry of Norrish Type-I Reactions: I. Experimental and Theoretical Studies of Acetone and Related Ketones on the S1 Surface. *ChemPhysChem* **2001**, *2* (5), 273−293.
(9) Favero, L.; Granucci, G.; Persico, M. Dynamics of Acetone Photodissociation: A Surface Hopping Study. *Phys. Chem. Chem. Phys.* **2013**, *15* (47), 20651−20651.
(10) Chen, W.-K.; Ho, J.-W.; Cheng, P.-Y. *J. Phys. Chem. A* **2005**, *109* (31), 6805−6817.
(11) Chen, W.-K.; Cheng, P.-Y. Ultrafast Photodissociation Dynamics of Acetone at 195 nm: II. Unraveling Complex Three-Body Dissociation Dynamics by Femtosecond Time-Resolved Photofragment Translational Spectroscopy. *J. Phys. Chem. A* **2005**, *109* (31), 6818−6829.
(12) Couch, D. E.; Kapteyn, H. C.; Murnane, M. M.; Peters, W. K. Uncovering Highly-Excited State Mixing in Acetone Using Ultrafast VUV Pulses and Coincidence Imaging Techniques. *J. Phys. Chem. A* **2017**, *121*, 2361−2366.
(13) Hüter, O.; Temps, F. Ultrafast α-CC Bond Cleavage of Acetone upon Excitation to 3p and 3d Rydberg States by Femtosecond Time-Resolved Photoelectron Imaging. *J. Chem. Phys.* **2016**, *145* (21), 214312−214312.
(14) Farmanara, P.; Stert, V.; Radloff, W. Ultrafast Photodissociation Dynamics of Acetone Excited by Femtosecond 155 nm Laser Pulses. *Chem. Phys. Lett.* **2000**, *320*, 697−702.
(15) Maierhofer, P.; Bainschab, M.; Thaler, B.; Heim, P.; Ernst, W. E.; Koch, M. Disentangling Multichannel Photodissociation Dynamics in Acetone by Time-Resolved Photoelectron-Photoion Coincidence Spectroscopy. *J. Phys. Chem. A* **2016**, *120* (32), 6418−6423.
(16) Rusteika, N.; Moeller, K. B.; Solling, T. I. New Insights on the Photodynamics of Acetone Excited with 253−288nm Femtosecond Pulses. *Chem. Phys. Lett.* **2008**, *461* (4−6), 193−197.
(17) Koch, M.; Heim, P.; Thaler, B.; Kitzler, M.; Ernst, W. E. Direct Observation of a Photochemical Activation Energy: A Case Study of Acetone Photodissociation. *J. Phys. B: At., Mol. Opt. Phys.* **2017**, *50*, 125102.
(18) Wilkinson, I.; Boguslavskiy, A. E.; Mikosch, J.; Bertrand, J. B.; Wörner, H. J.; Villeneuve, D. M.; Spanner, M.; Patchkovskii, S.; Stolow, A. Excited State Dynamics in SO_2. I. Bound State Relaxation Studied by Time-Resolved Photoelectron-Photoion Coincidence Spectroscopy. *J. Chem. Phys.* **2014**, *140* (20), 204301−204301.
(19) Brogaard, R. Y.; Sølling, T. I.; Møller, K. B. Initial Dynamics of the Norrish Type I Reaction in Acetone: Probing Wave Packet Motion. *J. Phys. Chem. A* **2011**, *115* (5), 556−561.
(20) Trebino, R.; DeLong, K. W.; Fittinghoff, D. N.; Sweetser, J. N.; Krumbügel, M. A.; Richman, B. A.; Kane, D. J. Measuring Ultrashort Laser Pulses in the Time-Frequency Domain Using Frequency-Resolved Optical Gating. *Rev. Sci. Instrum.* **1997**, *68* (9), 3277−3295.
(21) Koch, M.; Wolf, T. J. A.; Grilj, J.; Sistrunk, E.; Gühr, M. Femtosecond Photoelectron and Photoion Spectrometer with Vacuum Ultraviolet Probe Pulses. *J. Electron Spectrosc. Relat. Phenom.* **2014**, *197* (0), 22−29.
(22) Gregory, P. *Bayesian Logical Data Analysis for the Physical Sciences: A Comparative Approach with Mathematica® Support*; Cambridge University Press: 2005.
(23) Wu, G.; Boguslavskiy, A. E.; Schalk, O.; Schuurman, M. S.; Stolow, A. Ultrafast Non-Adiabatic Dynamics of Methyl Substituted Ethylenes: The π3s Rydberg State. *J. Chem. Phys.* **2011**, *135* (16), 164309.
(24) Shastri, A.; Singh, P. J. Vibrational Modes in Excited Rydberg States of Acetone: A Computational Study. *J. Quant. Spectrosc. Radiat. Transfer* **2016**, *173*, 92−105.
(25) Nobre, M.; Fernandes, A.; Ferreira da Silva, F.; Antunes, R.; Almeida, D.; Kokhan, V.; Hoffmann, S. V.; Mason, N. J.; Eden, S.; Limao-Vieira, P. The VUV Electronic Spectroscopy of Acetone Studied by Synchrotron Radiation. *Phys. Chem. Chem. Phys.* **2008**, *10* (4), 550−560.
(26) Shastri, A.; Singh, P. J.; Raja Sekhar, B. N.; D'Souza, R.; Jagatap, B. N. The Role of Torsional Modes in the Electronic Absorption Spectrum of Acetone. *J. Quant. Spectrosc. Radiat. Transfer* **2012**, *113* (12), 1553−1565.
(27) Domcke, W.; Yarkony, D. R.; Köppel, H. *Conical Intersections: Theory, Computation and Experiment*; Advanced series in physical chemistry; World Scientific Publishing Company: 2011.
(28) Ashfold, M. N. R.; Lambert, I. R.; Mordaunt, D. H.; Morley, G. P.; Western, C. M. Photofragment Translational Spectroscopy. *J. Phys. Chem.* **1992**, *96* (7), 2938−2949.
(29) Ashfold, M. N. R.; Murdock, D.; Oliver, T. A. A. Molecular Photofragmentation Dynamics in the Gas and Condensed Phases. *Annu. Rev. Phys. Chem.* **2017**, *68*, 63−82.
(30) Yarkony, D. R. *J. Chem. Phys.* **2005**, *122* (8), 084316.
(31) Karpichev, B.; Edwards, L. W.; Wei, J.; Reisler, H. Electronic Spectroscopy and Photodissociation Dynamics of the 1-Hydroxyethyl Radical CH_3CHOH. *J. Phys. Chem. A* **2008**, *112* (3), 412−418.
(32) Roberts, G. M.; Hadden, D. J.; Bergendahl, L. T.; Wenge, A. M.; Harris, S. J.; Karsili, T. N. V.; Ashfold, M. N. R.; Paterson, M. J.; Stavros, V. G. Exploring Quantum Phenomena and Vibrational Control in σ^* Mediated Photochemistry. *Chem. Sci.* **2013**, *4* (3), 993−1001.
(33) Bach, A.; Hutchison, J. M.; Holiday, R. J.; Crim, F. F. Competition between Adiabatic and Nonadiabatic Pathways in the Photodissociation of Vibrationally Excited Ammonia. *J. Phys. Chem. A* **2003**, *107* (49), 10490−10496.
(34) Hause, M. L.; Yoon, Y. H.; Crim, F. F. Vibrationally Mediated Photodissociation of Ammonia: The Influence of N-H Stretching Vibrations on Passage through Conical Intersections. *J. Chem. Phys.* **2006**, *125* (17), 174309.
(35) Hause, M. L.; Heidi Yoon, Y.; Case, A. S.; Crim, F. F. Dynamics at Conical Intersections: The Influence of O-H Stretching Vibrations on the Photodissociation of Phenol. *J. Chem. Phys.* **2008**, *128* (10), 104307.
(36) Lim, J. S.; Kim, S. K. Experimental Probing of Conical Intersection Dynamics in the Photodissociation of Thioanisole. *Nat. Chem.* **2010**, *2* (8), 627−632.
(37) Epshtein, M.; Yifrach, Y.; Portnov, A.; Bar, I. Control of Nonadiabatic Passage through a Conical Intersection by a Dynamic Resonance. *J. Phys. Chem. Lett.* **2016**, *7* (9), 1717−1724.
(38) Mai, S.; Marquetand, P.; Gonzalez, L. A General Method to Describe Intersystem Crossing Dynamics in Trajectory Surface Hopping. *Int. J. Quantum Chem.* **2015**, *115* (18), 1215−1231.

DOI: 10.1021/acs.jpca.7b05012
J. Phys. Chem. A 2017, 121, 6398−6404